Motion Analysis for Experimental Evaluation of an Event-Driven FES System

Andrea Prestia, *Graduate Student Member, IEEE*, Fabio Rossi, *Member, IEEE*, Andrea Mongardi, *Member, IEEE*, Paolo Motto Ros, *Member, IEEE*, Massimo Ruo Roch, *Member, IEEE*, Maurizio Martina, *Senior Member, IEEE*, and Danilo Demarchi, *Senior Member, IEEE*

***Abstract*— In this work, a system for controlling Functional Electrical Stimulation (FES) has been experimentally evaluated. The peculiarity of the system is to use an event-driven approach to modulate stimulation intensity, instead of the typical feature extraction of surface ElectroMyoGraphic (sEMG) signal. To validate our methodology, the system capability to control FES was tested on a population of 17 subjects, reproducing 6 different movements. Limbs trajectories were acquired using a gold standard motion tracking tool. The implemented segmentation algorithm has been detailed, together with the designed experimental protocol. A motion analysis was performed through a multi-parametric evaluation, including the extraction of features such as the trajectory area and the movement velocity.**

The obtained results show a median cross-correlation coefficient of 0.910 and a median delay of 800 ms, between each couple of voluntary and stimulated exercise, making our system comparable w.r.t. state-of-the-art works. Furthermore, a 97.39 % successful rate on movement replication demonstrates the feasibility of the system for rehabilitation purposes.

***Index Terms*— Event-driven, Experimental Protocol, Functional Electrical Stimulation, Motion Analysis, Surface Electromyography**

I. Introduction

Muscle paralysis is a condition able to gravely compromise the quality of life. This illness induces several limitations to the self-sufficiency, social integration, and psychological discomfort [1], [2]. The leading causes of paralysis are stroke, spinal cord injury, and multiple sclerosis [3]. These neurological deficits afflict the nervous system by inhibiting the ability of the brain to generate motor commands [4] or by compromising the neural pathway to the muscles [5], [6]. If the neurons innervating the skeletal muscles, together with the articular joints, are still functional, the contraction of the myofibers can be induced through Functional Electrical Stimulation (FES) [7]. FES consists in applying low energy pulses to the axons of motor neurons for action potentials generation [7]. The primary aim of the FES is to restore the movements functionalities, but also to improve blood circulation and prevent muscle atrophy due to disuse [8].

Different strategies can be employed to control FES, either by triggering the stimulation, or by modulating the energy of the stimulation pulses [9], [10]. If the control aims to be at a central level, the ElectroEncephaloGraphy (EEG) can be used by integrating FES into a Brain-Computer Interface (BCI) and exploiting approaches such as Motor Imagery (MI) [11] or Action Observation Treatment (AOT) [12]. Alternatively, focusing on a peripheral level control, surface ElectroMyoGraphy (sEMG) could be employed to build a Human-Machine Interface (HMI) [13] thanks to its widespread adoption in monitoring skeletal muscle activity for both the diagnostics and prosthetic fields [14], [15].

Among the mentioned techniques, we opted for an sEMG-FES system because it directly activates the muscle fibers by processing the information of the muscular activation itself, thus avoiding more complex feature extraction from EEG. Moreover, similar to FES, sEMG works with surface electrodes easily placed on the muscle belly, allowing the overall system to be completely non-invasive and fast to set up. In this scenario, the muscles from which the sEMG signals are acquired can be contralateral of the stimulated ones, or they can be muscles belonging to a different person from the one receiving the stimulation. In the first case, known as Contralaterally Controlled FES (CCFES) [9], the controller and the controllee are the same subject, and this self-stimulation is growing interest for the therapeutic management of hemiplegia and hemiparesis. In the second case, the stimulation applied to a patient is modulated by processing the muscular activity of a therapist, intended as a professional capable of performing a physiologically ideal movement [16]. Moreover, the efficacy of the therapist-controlled FES approach could be further improved by allowing the patient to see the therapist during the movement execution. Indeed, as in AOT rehabilitation protocols, the involvement of mirror neurons, which fire during the observation of an action, promotes neural plasticity [17], [18].

Looking at the recent state-of-the-art, sEMG parameters such as the signal envelope [19]–[21] or its entropy [22] are typically used to define the stimulation pattern. Further approaches involve extracting multiple time-domain features (e.g., mean absolute value, zero-crossing, number of slope sign changes) to feed a machine learning algorithm for FES parameters modulation [23], [24]. However, the features processing requires the full recording of the sEMG signal, followed by software extraction techniques. Finding a way to relax these computations, we proposed a completely different approach, named Average Threshold Crossing (ATC) [25],

Date of current version: December 17, 2021. Corresponding author is Andrea Prestia; email: andrea.prestia@polito.it

All the authors are with Department of Electronics and Telecommunications, Politecnico di Torino, 10129 Turin, Italy.

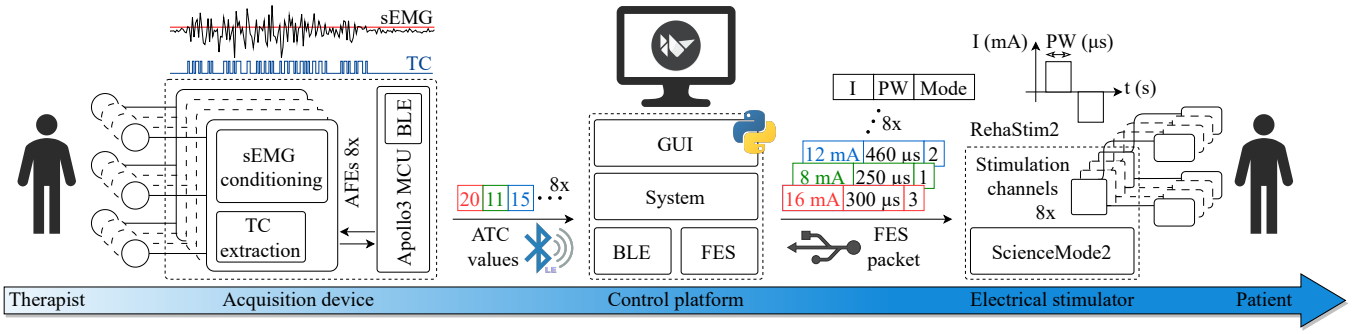

Fig. 1: The main use-case scenario consists in the following information flow. (**left**) The therapist performs a movement while wearing the acquisition device. Each AFE consists of the sEMG signal conditioning stages and the voltage comparator for the Threshold Crossing (TC) signal generation. All the AFEs (up to 8, as the stimulation channels) are connected to the Apollo3 MicroController Unit (MCU) to count the TC events (i.e., calculating ATC) and stream the ATC values through its Bluetooth Low Energy (BLE) transceiver. (**middle**) The control platform, whose modular software is developed using the Python programming language, receives the ATC values and processes them to define the stimulation parameters. The user can actively supervise the system functionalities (e.g., active channels selection, plotting of ATC and FES values) by interacting with a custom Graphical User Interface (GUI). (**right**) The electrical stimulator (RehaStim2) receives commands from the control platform via serial communication and applies FES to the patient for movement replication.

which does not even require sampling the sEMG signal. Our process consists of counting how many times the analog sEMG signal overcomes a threshold in a period (i.e., ATC window). Considering the demonstrated relation between ATC and muscle activity [26], this approach results in an on-board feature extraction process suitable for edge-computing applications [27], [28]. Indeed, taking into consideration the FES scenario, in our recent work [29], we described how the ATC-FES definition could be implemented using a very simple Look-Up-Table (LUT) structure, which allows us to achieve, among all, promising results from a real-time application perspective (i.e., processing time below 10 ms).

In this paper, being aware of the electronic robustness of our system, we took a further step toward the validation of the ATC-FES prototype, aiming to confirm the previous and introductory motor tests [30]. A novel experimental campaign has been conceived by involving 17 healthy subjects in simulating therapist-patient rehabilitative sessions for upper and lower body limb flexion and extension. A motion capture system has been used to record voluntary and stimulated movements to assess their similarity. We developed a trajectories analysis algorithm to extract well-known figures of merits (e.g., cross-correlation, delay) and new experimental ones (e.g., area, velocity) to evaluate the ATC-FES motor control performance.

Although the analyzed movements are still a simplistic representation of daily-life actions, our starting point gave us feedback on the pros and cons of our system, and set a reference point for next analyses about more complex movements and tests on pathological subjects.

II. Materials and Methods

The system architecture, whose high-level block-scheme is depicted in Fig. 1, is composed of the acquisition device, the control platform, and the electrical stimulator. In the main use-case scenario, the execution of a movement by the therapist, from which the sEMG signals are acquired, results in the replication of the same movement by the patient, to which FES is applied [16]. Basically, the acquisition device applies the ATC technique to the sEMG signals and transmits the ATC values through Bluetooth Low Energy (BLE) communication [27]. On the basis of the ATC values, the control platform computes a suitable stimulation intensity pattern (i.e., modulating the pulse amplitude) to allow the stimulated patient to replicate the therapist movement in a bio-mimetic way [29]. Dedicated experimental tests allowed us to evaluate system performances in terms of therapist-patient (subjects) movements replicability.

A. System architecture

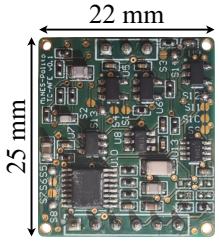

Fig. 2: AFE.

1) Acquisition device: Considering our previous experiences in implementing ATC-FES systems [27], [29], [30], we developed an improved version of our acquisition device architecture [28], [29] able to fit at best our needs. The proposed solution consists of multiple Analog Front Ends (AFEs), which properly detect sEMG raw signals and extract Threshold Crossing (TC) events, and a digital part for ATC computation and data transmission (see Fig. 1 (left)). The AFE architecture (Fig. 2 shows a prototype) is the evolution of the channel described in [29]: the sEMG conditioning circuit is designed for differential signal acquisition (i.e., two sensing electrodes and one which refers a common electrical potential [31]), providing a 70 Hz–400 Hz transfer function with a default gain of 500 V/V (which could be further increased by $\times 2$, $\times 3$, $\times 5$ or $\times 6$ multiplication factor if needed). The last stage of each AFE is a voltage comparator, which, by applying a calibrated threshold to the analog sEMG signal, allows the generation of the quasi-digital TC signal [25]. This final output is then provided to the MCU for ATC computation.

After different investigations in defining the most efficient digital configuration [25], [27]–[29], we selected the Apollo3 Blue [32] MCU because of its ultra-low power features for embedded computing, which also simplify the design of portable and wearable battery-powered acquisition devices.

A BLE server was implemented on the acquisition side making the system easy to be interfaced and supervised: beyond the configurable features (e.g., programmable gain, threshold setting for ATC), the device streams ATC values every 130 ms [25] to the control platform client.

2) Control platform and software: The inputs/outputs of the system are commonly handled by a laptop, but, alternatively, a Raspberry Pi can be employed [29]. The control software was developed using the Python programming language, and it is designed on three levels (see Fig. 1 (middle)). At the bottom level, the BLE and FES modules are dedicated to communication with the Bluetooth acquisition device and the electrical stimulator (USB interface), respectively. At the middle level, the System module processes in real-time the ATC data received from the BLE module to generate a suitable stimulation pattern for FES. The use of minimal information (i.e., ATC) allows us to condense the processing phase in a LUT that links, for each acquisition/stimulation channel, the ATC value with the stimulation intensity, as reported in [29]. Finally, at the top level, a Graphical User Interface (GUI) was designed to guarantee full (and secure) control over FES.

3) Electrical stimulator: As in the previous works [27], [29], [30], we continued to use the RehaStim 2 [8] as electrical stimulator considering its enhanced features: its battery power-supply minimizes noise interference (e.g., 50 Hz power-line); the symmetrical bi-phasic pulse pattern avoids charge accumulation in stimulated tissues; many configurable parameters permit the user to achieve an improved FES modulation of up to 8 channels simultaneously, also adapting the stimulation to subject(s) body conditions. The control of the device is via the ScienceMode2 communication protocol [33], whose convenient implementation allows the user to update the stimulation parameters (e.g., pulse amplitude, pulse width, pulse group mode) during on-going stimulation (see Fig. 1 (right)). In the developed system, this protocol perfectly meets our need to update the stimulation intensity (i.e., pulse amplitude) every time new ATC values are available (at the end of each 130 ms window) [29].

B. Experimental protocol

The effectiveness of the proposed ATC-FES motor control was investigated simulating clinical rehabilitative sessions. In particular, during the experimental campaign, we focused on the therapist-patient configuration, instead of the self-stimulation approach (i.e., CCFES), to promote the muscular relaxation of the stimulated subject, which could not be entirely achieved if the same subject is already executing another movement. Each test involved two subjects: the therapist performs the movement voluntarily and the patient replicates the movements as a consequence of FES application. In this situation, ATC values expressed by the therapist were used in the definition of FES intensity. From these tests, we aimed to extract the trajectory of the voluntary and stimulated movements and compare them to analyze their similarity. Therefore, subjects body movements were captured using the Vicon system in a 12 camera configuration, as it is the commercial gold standard tool for motion capture [34]. Investigating clinical procedures and state-of-the-art works [24], [35]–[38], we defined a total of six key movements concerning both upper and lower limbs, listed below with their reference positions:

- Elbow Flexion (EF): subjects are seated with the forearm in supine position and the elbow leaning on the table. Among analyzed movements, this is the one with the highest Range Of Motion (ROM) [39], [40].
- Wrist Extension (WE): subjects are seated with the forearm in neutral position and the elbow leaning on the table.
- Wrist Flexion (WF): same reference position of WE.
- Knee Extension (KE): subjects are seated on a chair high enough to avoid any impairment between the foot and the floor during movement execution. Among analyzed movements, this is the one with the greatest load, given by the weight of the lower leg.
- Ankle Extension (AE): same reference position of KE. Among analyzed movements, this is the one with the lowest ROM [39], [40].
- Ankle Flexion (AF): same reference position of KE.

The test campaign involved a total of 17 healthy volunteers, 12 males and 5 females, aged between 24 and 30 years old.

In compliance with regulations regarding COVID-19, the proper distance between the subjects was guaranteed and each of them was required to wear a protective mask. The sanitizer gel was used during the preparation phase of the subjects and it was made available for further use.

These experimental tests were approved by the Comitato Bioetico di Ateneo of the University of Turin [41] (experimental code: 445154).

In the following paragraphs, the phases of our experimental test are described.

1) Procedures explanation: The goal of the test and how it would be performed were explained to the volunteers, also detailing technical information about the instrumentation. The informed consent signature was required from participants to proceed with the testing phase.

2) Vicon system setup: After placing all the necessary equipment in the 3D motion capture environment, Vicon infrared cameras were masked to limit instrumentation reflection, which could lead to data corruption [42]. Then, the sampling volume was calibrated and the axes' origin was set. Reflective markers were applied to subjects' bodies following the positioning guideline reported in [43]. In particular, considering that our tests concerned only upper and lower limbs, we limited the applied markers to those needed for our experimental campaign, hence excluding head, torso, and pelvis areas.

3) Electrodes application: Kendall™ H124SG (Ag/AgCl, 24 mm ⌀) pre-gelled electrodes [47] were used for sEMG detection. The SENIAM project recommendations [44] were followed to adequately prepare the skin before electrodes

attachments, preventing the sEMG signal to be corrupted by noise sources (e.g., motion artifacts) or electrodes imbalance. Electrodes locations were identified both considering SENIAM project indications [44] and through manual palpation, thus assuring the correct and standardized placement w.r.t. the muscles condition of involved subjects.

As regards the stimulation electrodes, we employed the HASOMED® RehaTrode [8] (5 cm×9 cm) and the FIAB PG470W [48] (3.5 cm×4.5 cm) products to provide the appropriate stimulation intensity considering the diverse typology and orientation of muscle fibers. As for sEMG, skin preparation and standardization of electrode placement were provided following the indications reported in [45] and [46], also taking care to apply a conductive gel on electrode surface to enhance the current flow and to minimize discomfort perception.

A summary of the acquisition and stimulation muscles, and their relative electrode locations, are listed in Table I. These indications are not strictly binding, since depending on the subjects' anatomy and their comfort with stimulation, the positioning can be modified.

4) ATC-FES system calibration: The creation of the ATC-FES relationship by means of the LUT structure [29] allows the system to completely exploit its versatility, making possible the adaptation of the physiological muscle conditions (e.g., muscular tone, exerted force) among subjects. At the end of this two-step process, the therapist ATC values drive a stimulation intensity (i.e., pulse amplitude) able to reproduce a similar action in the patient body, although their different muscle status.

The first step includes the calibration of the ATC threshold during the muscular rest condition and the subsequent repetition (at least three times) of the desired movement in order to identify the maximal variation of the ATC value.

In the second step, the maximal value of the stimulation intensity, able to induce the target action in the patient, is determined. To accomplish this task, the stimulation intensity is gradually increased until the proper setting is identified. If the subject feels discomfort (e.g., cramp, burning or pain), non-modulated stimulation parameters (i.e., frequency, pulse width) or the electrodes position could be changed trying to better adapt to subject condition.

5) Test execution: Every trial consists of three sessions, during which each target movement is repeated ten times, preserving 10 s inter-repetition and 5 min inter-session pause times to prevent muscle fatigue effects.

Since each type of movement was performed by 8 volunteers at least, with the exception of WF with 9 volunteers (because not all the subjects had the time availability to participate in testing all the six movements), we obtained a minimum number of 240 repetition for each movement.

The selected stimulation frequency (f_s) and pulse width (PW) for each movement, employed during the calibration and execution phases, are reported in the right columns of Table I.

Fig. 3 (top) shows our experimental setup for upper limbs movements, where the two subjects are positioned frontally with the electrodes and markers applied. The reference position features the subjects sitting upright with the limbs aligned. In Fig. 3 (middle) an example of the reconstruction of body segments for upper limbs, thanks to the identification of Vicon markers, is reported. The angular trajectories of both subjects are accordingly extracted, as represented in Fig. 3 (bottom).

C. Data processing

The sampling frequency of Vicon cameras was set to 100 Hz, a suitable value to accurately reconstruct human joint flexions and extensions [49]. Starting from markers identification and human body segments reconstruction, limb trajectories were extracted using the Nexus software [50]. Since the Vicon cameras may not recognize some markers during the execution of the test, data interpolation was often needed to reconstruct the totality of the rigid body. At this point, movements trajectories were obtained by running the Kinfit tool of the Nexus software, which, by processing markers coordinates, results in the extraction of 3D volume trajectories.

Vicon data were further processed on MATLAB®. Preprocessing steps include the discard of segments that do not belong to the test execution, and signal sign adjustment in order to match the system reference for the two acquired trajectories. Then, a segmentation process was performed to identify four temporal coordinates for each movement repetition: the start (s_1) and the end (s_2) of the rise; the start (s_3) and the end (s_4) of the fall (see Fig. 4). Basically, the implemented segmentation algorithm scans for variations in the derivative

TABLE I: For each tested movement, the acquisition and stimulation sites are reported, together with the involved muscles. The non-modulated stimulation parameters used during the experimental tests are also shown.

ID	Acq. muscles	Acquisition sites[1,3]	Stim. muscles	Stimulation sites[2,3]	f_s[2,3] (Hz)	PW[2,3] (µs)
EF	*Biceps Brachii*	Line *medial acromion - fossa cubit* at 1/3 from *fossa cubit*	*Biceps Brachii*	E1: closer to the crease of the elbow, E2: over the muscle belly	40	250 - 350
WE	*Extensor Carpi Ulnaris*	At 10 % of line *medial epicondyle of the humerus - ulnar styloid process*	*Extensor Carpi Ulnaris, Extensor Digitorum*	E1: over the tendinous area of the forearm, E2: just distal to lateral condyle	40	200 - 300
WF	*Flexor Carpi Radialis*	At 10 % of line *medial epicondyle of the humerus - radial styloid process*	*Flexor Carpi Radialis, Palmaris Longus*	E1: over the flexor surface of tendons, E2: high towards the medial condyle	40	200 - 300
KE	*Rectus Femoris*	At 50 % of line *anterior spina iliaca superior - superior part of patella*	*Quadriceps Femoris*	E1: proximal and towards the lateral side, E2: distal and slightly to the medial side	40	350 - 500
AE	*Gastrocnemius*	At 1/3 of line *head of fibula - heel*	*Gastrocnemius, Soleus*	E1: over the origins of both the medial and the lateral gastrocnemius, E2: over the soleus	40	300 - 400
AF	*Tibialis Anterior*	At 1/3 of line *tip of fibula - tip of medial malleolus*	*Tibialis Anterior, Peroneus*	E1: close to the tibia, further down the shank, E2: over the muscle belly, very midline	40	250 - 300

[1]Compliant with [44]; [2]Compliant with [45], [46]; [3]Adjustable to account for variability across subjects.

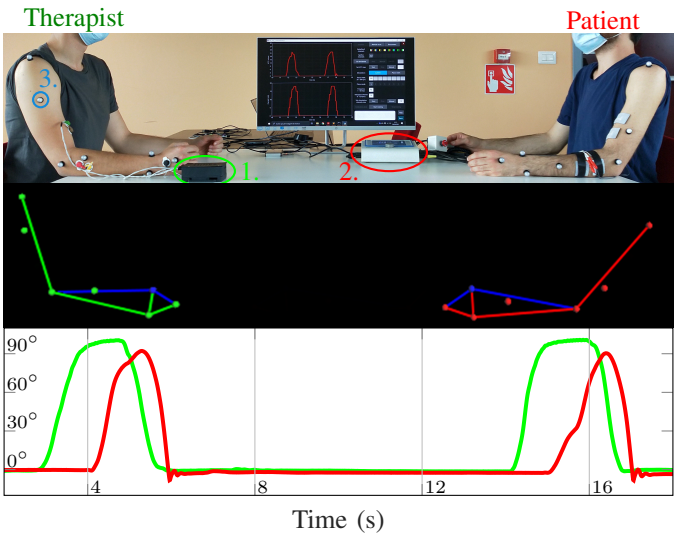

Fig. 3: (**top**) Experimental setup: the therapist (on the left) and the patient (on the right) are connected to the acquisition device (1) and the electrical stimulator (2), respectively; Vicon markers (3) are applied on both subjects; (**middle**) Upper limbs reconstruction using Vicon system; (**bottom**) Exported elbow flexion trajectories.

of the signal. The algorithm is provided with the following parameters: Diff_{min} is the minimum signal variation for rising and falling points definition; N_{s_1,s_4} and N_{s_2,s_3} are the number of analyzed consecutive points to identify s_1 and s_4, or s_2 and s_3, respectively. For the identification of s_1 and s_4, N_{agree} and N_{disagree} are also used, both percentages relative to N_{s_1,s_4}: N_{agree} defines the minimum number of points that must be consistent with the identification (e.g., in the case of s_1 the subsequent points must be rising ones); N_{disagree} defines the maximum number of allowed contrary points (e.g., the maximum number of falling points in the rising phase).

The steps of the segmentation algorithm are summarized in the following list:

1) Application of a moving median operator, with window length equal to 41 samples, to suppress the noise resulting from possible markers flickering (which can be present despite Nexus interpolation) and to allow the algorithm to neglect the non-relevant signal fluctuations, such as those resulting from the return of the limb to its reference position (see Fig. 4 (a), at 2.8 s);
2) Down-sampling of the signal by $\times 2$ factor to simplify the segmentation process, as it depends on the number of points in the trajectory and the difference of their values (this step is not strictly necessary, but a high sampling rate is not required for segmentation and a lower rate makes the choice of tuning parameters less critical);
3) Identification of the rising and falling points of the trajectory by applying a threshold (i.e., Diff_{min}) to the derivative of the signal, as reported in Equation 1:

$$p_i \in \begin{cases} Rising, & \text{if } p_i - p_{i-1} \geq \text{Diff}_{\text{min}} \\ Falling, & \text{if } p_i - p_{i-1} \leq -\text{Diff}_{\text{min}} \end{cases} \quad (1)$$

where p_i is the i-th point of trajectory.

4) Moving forward on the signal one point at a time; if the current point is a rising one, and at least the N_{agree} percent of the next N_{s_1,s_4} points are rising point, and less than the N_{disagree} percent of them are falling points, then the current point is identified as s_1;
5) Moving backward on the signal one point at a time (starting five seconds after s_1), if the current point is a falling one, and at least the N_{agree} percent of the next N_{s_1,s_4} points are falling point, and less than the N_{disagree} percent of them are rising points, then the current point is identified as s_4;
6) Identification of the maximum value between s_1 and s_4;
7) Starting from the 70% of the maximum value (left side), moving forward one point at a time, if the current point is a rising point, and there is at least one rising point among the next N_{s_2,s_3} points, then the current point is identified as s_2. If s_2 is not identified within the maximum point, s_2 is located at the point before the maximum point;
8) Starting from the 70% of the maximum value (right side), moving backward one point at a time, if the current point is a falling point, and there is at least one falling point among the next N_{s_2,s_3} points, then the current point is identified as s_3. If s_3 is not identified within the maximum point, s_3 is located at the point after the maximum point.

Due to the variability among acquired trajectories, the parameters of the algorithm can vary slightly between different movements. Table II reports the typically used values, which, although not constraining, can be used as reference. Still, it is up to the user to determine the most appropriate ones.

The alterations made to the signal during processing (e.g., down-sampling) regard only the segmentation algorithm, while the extraction of the evaluation features (described below) is carried out on the original signal, to which just a moving median operation with window length equal to 11 samples is applied for noise suppression.

In the formulas below for calculating the evaluation features, $e_{k,x}$ and $t_{k,x}$ are the excursion and time components of the k-th sample of the therapist (x = *'th'*) or patient (x = *'pt'*) trajectory.

In order to test the performances of the system, the normalized cross-correlation coefficient (ρ) and the delay (D) between therapist and patient movements were computed to evaluate the effectiveness of the FES control, as also reported in [23], [51]. While ρ perfectly represents the similarity among

TABLE II: Typical parameters tuning for the trajectories segmentation algorithm.

ID	Diff_{min} (°)	N_{s_1,s_4}	N_{s_2,s_3}	N_{agree} (%)	N_{disagree} (%)
EF	0.8	10	7	70	20
WE	0.6	10	7	70	20
WF	0.4	12	9	70	20
KE	0.6	10	7	70	15
AE	0.2	10	7	50	20
AF	0.4	12	7	50	20

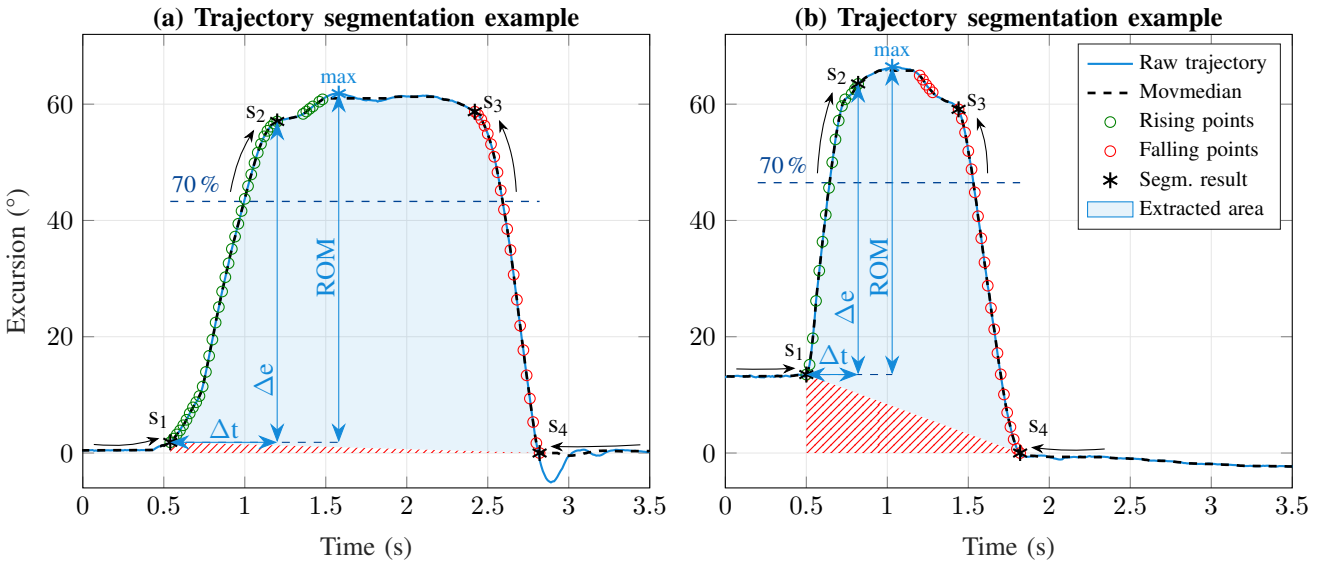

Fig. 4: The example (a), on the left, reports a trajectory with no significant baseline changes between the beginning and end of the movement, in contrast to the trajectory shown on the right (b). Starting from the rising (green) and falling (red) points of the curve, we obtain s_1, s_2, s_3, and s_4, which are the segmentation result. Using them, we extract the evaluation parameters of interest ($\rho_{\max}$, D, ROM, v, and A) for each movement repetition. Section II-C provides for more detailed information about the segmentation algorithm and the formulas used for parameters extraction.

movements, from D we obtained an overall information about FES application timings, including both computational and physiological latencies. Moreover, we computed ρ also between the subjects trajectories and their respective ATC and FES profiles to better understand the most critical step during the transfer of information (see the information flow from therapist to patient in Fig. 1). Equations 2 and 3 show the formulas for $\rho_{\max}$ and D:

$$\rho_{\max} = \max\big(\rho(m)\big) = \max\left(\frac{\hat{R}_{a,b}(m)}{\sqrt{\hat{R}_{a,a}(0)\hat{R}_{b,b}(0)}}\right) \tag{2}$$

$$D = t_{s_1,pt} - t_{s_1,th} \tag{3}$$

where $\hat{R}_{a,b}$ is the estimated correlation between a and b (i.e., therapist or patient trajectory, ATC or FES profile) and m is the lag between the signals.

We also performed a complementary analysis by calculating Range Of Motion (ROM), rise velocity (v) (i.e., the velocity of the concentric phase of the movement), and area under the curve (A). We deemed the use of these three trajectory features effective to complete the qualitative analysis about the executed movements. Fall velocity (i.e., the velocity of the eccentric phase of the movement), on the other hand, was not taken into account since our focus is addressed to the active phase of the movement. Fig. 4 reports an example of our segmentation results, also providing a figurative concept of the extracted parameters, which were computed as follows:

$$ROM_x = e_{\max,x} - e_{s_1,x} \tag{4}$$

$$v_x = \frac{\Delta e}{\Delta t} = \frac{e_{s_2,x} - e_{s_1,x}}{t_{s_2,x} - t_{s_1,x}} \tag{5}$$

$$A_x = \sum_{i=s_1}^{s_4} \Big(e_{i,x} - \min\left(e_{s_1,x}, e_{s_4,x}\right)\Big) \cdot t_s + \\ - \frac{|e_{s_4,x} - e_{s_1,x}| \cdot (t_{s_4,x} - t_{s_1,x})}{2} \tag{6}$$

where t_s is the Vicon sampling period (i.e., 10 ms).

In Equation 6, the subtraction of $\min\left(e_{s_1}, e_{s_4}\right)$ takes into account the possibility of negative excursion values caused by baseline oscillation. Indeed, after some movement repetitions, the baseline usually differs from zero because the subject does not always return to the starting reference position (see Fig. 4(b)). The second term of Equation 6 takes into consideration the effect of the baseline changes in terms of computed areas by removing over-estimation, as depicted by red dashed area in Fig. 4.

In order to evaluate relative, rather than absolute, quantities, parameters ROM, v, and A extracted from each patient movement are normalized to those obtained from the corresponding therapist one as reported in Equation 7. Therefore, each parameter is referenced to the maximum ROM value obtained from each subject to consider her/his maximum excursion capabilities.

$$X_{pt/th} = \frac{X_{pt}}{X_{th}} \cdot \frac{\max(ROM_{th})}{\max(ROM_{pt})} \tag{7}$$

where X can be ROM, v, or A.

III. Results and Discussion

This section reports the results, and their discussion, which allowed us to reach a proper evaluation of the proposed system. We report our experimental analysis about the voluntary and stimulated movements replication, discussing the appropriateness of our approach w.r.t. the descriptive parameters we

TABLE III: Extracted parameters for motion assessment.

Param.	Description
$\rho_{\max}$	Maximum normalized cross-correlation coefficient
D	Delay between therapist and patient movement
ROM	Movement excursion
v	Limb velocity during concentric phase
A	Area under angular trajectory
SR	Successful rate of movement replications

extracted from the limbs trajectories. Table III summarizes the evaluation parameters used for the following discussion.

Fig. 5 and 6 show our comparison analysis, between the therapist and patient angular data, for all the extracted parameters (see Section II-C), which are organized into box plots to adequately represent the information variability of each movement along the total number of repetitions. Furthermore, we decided to synthesize our results using the median value because it adequately describes a population of measurements while being more robust (to the outliers) than the mean value.

Since our purpose is the real-time control over the stimulation, giving the possibility to the therapist to correct her/his movement according to the one executed by the patient, we measured the movement replication delays. Obtained values (see Fig. 5 (a)) are up to about 100 times higher than the computational latencies of the control software, which is typically within 10 ms [29]. Indeed, the latter has to be summed to the 130 ms of implicit delay due to the use of the window we chose for the ATC. In addition, the measured delay also includes the lag between the onset of the therapist movement and the first TC events indicating muscle activity. Finally, an additional delay component is the physiological

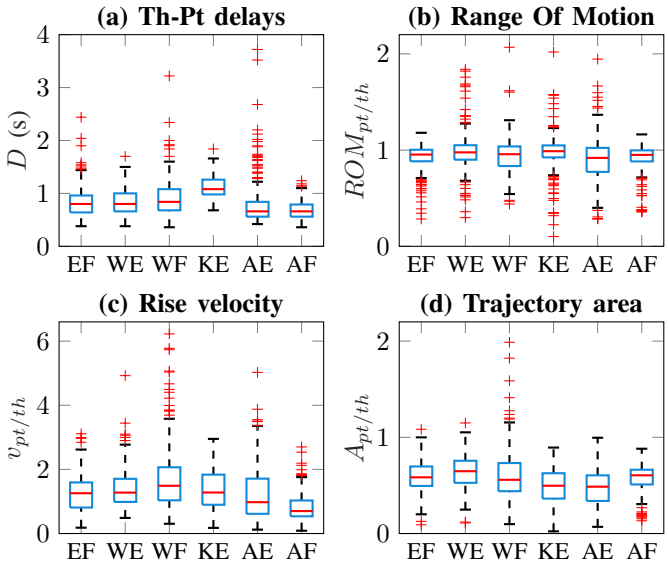

Fig. 5: Angular trajectories features comparison between therapist and patient movements: Elbow Flexion (EF), Wrist Extension (WE), Wrist Flexion (WF), Knee Extension (KE), Ankle Extension (AE), Ankle Flexion (AF). Please refer to Equation 7 to see the normalization performed for features with subscript pt/th.

response time between the start of the stimulation and the beginning of the movement, which in literature is known as ElectroMechanical Delay (EMD) [52], and can be over 300 ms [53]. The highest median value of replication delay, equal to 1.08 s, has been obtained during knee extension repetitions while the lowest results have been found for ankle flexion, calculating a median value equal to 660 ms. The significant difference between these two movements, which both act against gravity, is that the *tibialis anterior* muscle reaches its maximum activation values after few degrees of excursion, while the *quadriceps femoris* muscles are mainly activated during the last stages of excursion, when the load has the greatest weight. Following the above discussion, these delay values, with an overall median of 800 ms, are sufficiently low to allow the therapist to adjust and modulate her/his movement in response to the patient's activity. This possibility surely increases the application versatility of the proposed system since it gives the user the opportunity to control the stimulation during the session, e.g., updating the FES intensity to help the patient reach the target exercise according to the subject's physical abilities.

Looking at Fig. 5 (b), the median of the obtained $ROM_{pt/th}$ values is about 1 (0.92–0.99) for all movements. This can be justified by the fact that, in general, the protocol to which we adhered avoid a fatigue onset affecting the patient movement more than the therapist one, as the excursions were proportional between the two subjects. However, there is a discrete presence of outliers for knee and wrist extension, mainly due to less excursion by the patient. For knee extension, we found that these outliers are due to the lack of ATC values sufficiently high to generate a stimulation intensity suitable to complete the execution of the movement, which we recall to be the one with the greatest body load. This could be solved by adapting the calibration strategy to update the reference ATC values since, with the progress of the exercise, the therapist may express lower values than those obtained during the calibration phase. Instead, for wrist extension the outliers are related to the fact that, during our tests, each repetition of wrist extension did not alternate with a repetition of wrist flexion. Hence, sometimes the patient's wrist did not return to the same starting position, thus reducing the resulting ROM (see Fig. 4 (b)). In particular, we calculated that 4 % of wrist extension repetitions had a baseline drop greater than 20 % of the total excursion performed.

With the exception of ankle movements, the rise velocity comparison (Fig. 5 (c)) offered $v_{pt/th}$ with medians greater than 1: the movement of the patient, in fact, is typically faster than the one of the therapist due to stimulation. While for ankle extension the median $v_{pt/th}$ is equal to 0.98, for ankle flexion it is 0.70. A plausible explanation for having lower values for these movements is that the ankle joint is also the one with the lowest ROM among those analyzed: hence, both the subjects soon reach the maximum joint excursion.

The area comparison box plot (Fig. 5 (d)) shows median $A_{pt/th}$ values between 0.49 and 0.65 among the tested movements. Considering that the areas are normalized over the maximum ROM obtained from the respective subject, this comparison parameter is strictly dependent on the movement

replication delays. Indeed, the delay mainly affects the beginning of the movement, whereas the end of the activity of the two subjects is almost simultaneous (we calculated a median delay equal to 20 ms among all the performed repetitions). Moreover, the area offers an overall information given by the trajectory shape, thus being dependent also on rise velocity. In fact, ankle flexion and extension involve similar delays (both present median values equal to 660 ms) but this behavior is not reflected by $A_{pt/th}$ (median values equal to 0.48 for AE and 0.60 for AF). This aspect can be justified by looking at rise velocity box plot (Fig. 5 (c)), where ankle extension results in greater $v_{pt/th}$ values (median equal to 0.97 against 0.70 for AF), thus reducing the area under the curve.

The correlation for each step of the information transfer is reported in Fig. 6. As regards $\rho_{\max}$ between therapist trajectory and ATC profile (Fig. 6 (a)), the highest results have been obtained for wrist extension, ankle extension and ankle flexion, with the median of $\rho_{\max}$ equal to 0.950, 0.942, and 0.973, respectively. A considerable contribution to this fact is that, for these three cases, muscle activity is easily detectable during the whole execution of the movement, thus increasing the overlap between the therapist trajectory and the corresponding ATC profile. While for elbow flexion and wrist flexion the median of $\rho_{\max}$ is still quite high (0.927 and 0.905, respectively), for knee extension we obtained 0.862. In fact, as discussed above, the main activity occurs during the isometric phase of the KE movement, rather than during the concentric or eccentric one.

The median values of $\rho_{\max}$ among ATC and FES profiles (Fig. 6 (b)) are always higher than 0.970, since the only non-linearity during ATC processing is the moving median operation implemented for noise robustness. Also for the correlations between the FES profiles and the patients trajectories (Fig. 6 (c)) the computed values are quite high, although the presence of a greater number of outliers in cases where the stimulation parameters were not adequate for the proper execution of the movement.

For $\rho_{\max}$ among therapist and patient limb trajectories (Fig. 6 (d)), we chose an acceptability threshold equal to 0.850 as it is consistent with what is found in the literature [22], [23], [54]. The obtained median value among all the executed exercises is equal to 0.910, largely satisfying the chosen constraint. Going into details, the lowest result has been obtained for knee extension, with a median value of $\rho_{\max}$ equal to 0.861, as a consequence of what has been discussed before. The highest outcomes, instead, have been obtained during ankle extension and elbow flexion repetitions, with median values equal to 0.931 and 0.923, respectively. For ankle extension, such a high $\rho_{\max}$ is not surprising, since among the six proposed movements this is the simplest one, with the lowest excursion.

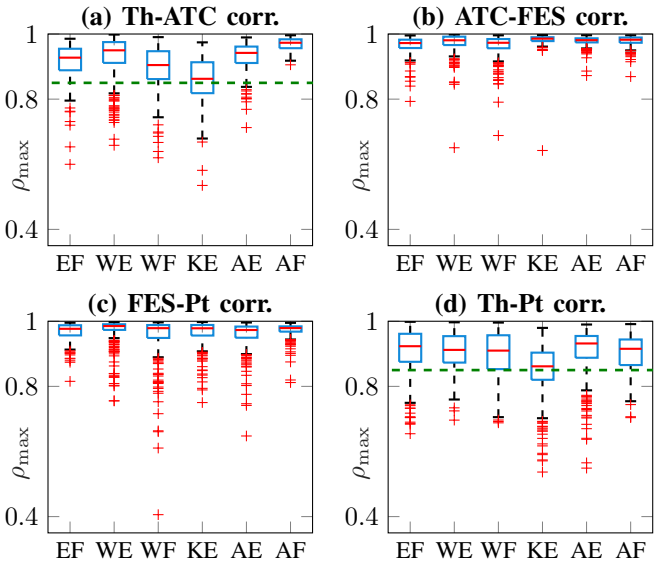

Fig. 6: Maximum of the cross-correlation coefficient ($\rho_{\max}$) for each step of the information flow, divided among movement types: Elbow Flexion (EF), Wrist Extension (WE), Wrist Flexion (WF), Knee Extension (KE), Ankle Extension (AE), Ankle Flexion (AF). The green dashed line at $\rho_{\max} = 0.850$ in (a) defines the threshold used for the classification of *ATC poor*, whereas in (d) indicates the selected acceptability threshold for the overall correlation (i.e., therapist and patient trajectories similarity).

In order to account also for movements not replicated by the patient, we labeled them according to the reason of the failures, as reported in Table IV. If the $\rho_{\max}$ between therapist trajectory and ATC profile is lower than 0.850, we classified the movement failed for *ATC poor*. Otherwise, if the failed movement is consecutive to a stimulation pattern with a maximum intensity 60 % lower than the stimulation value established during calibration, the movement is classified as *FES poor*. Lastly, if the failure of the movement is not ascribable to either of these two cases, the movement is classified as *FES ineffective*. From these labels, we defined the Successful Rate (*SR*) parameter as the number of valid repetitions over the total, to summarize the replication success for each tested movement. Even if the SR values are satisfactory for all the tests, it is interesting to note that elbow flexion and ankle extension are the movements with the lowest reproduction rate (below 97 %), although their (median) cross-correlation coefficient is the highest among all the movements.

TABLE IV: The total number of repetitions for each type of movement (e.g., EF, WE) has been analyzed to classify the replication outcome: a *valid* label means that the therapist and patient trajectories are almost similar; otherwise, an unsatisfactory replication of movements is marked as *ATC poor*, *FES poor*, or *FES ineffective* depending on the cause of failure. The Successful Rate (*SR*) is calculated as the percentage ratio between the valid and total movement repetitions.

ID	Total	Valid	ATC poor	FES poor	FES ineff	*SR* (%)
EF	273	263	7	2	1	96.34
WE	260	254	2	3	1	97.69
WF	290	282	1	5	2	97.24
KE	256	249	5	1	1	97.27
AE	264	255	3	1	5	96.59
AF	250	248	0	1	1	99.20

This final outcome, in addition to the above discussion, points out how a multi-parameters approach is needed to characterize an FES system effectively: the motor control and the movement reproduction could not be described simply by analyzing the cross-correlation coefficient among the therapist and patient trajectories, but additional parameters (e.g., area, velocity) and the evaluation of the FES definition process (i.e., Fig. 6) are essential to better understand the effectiveness of an induced movement.

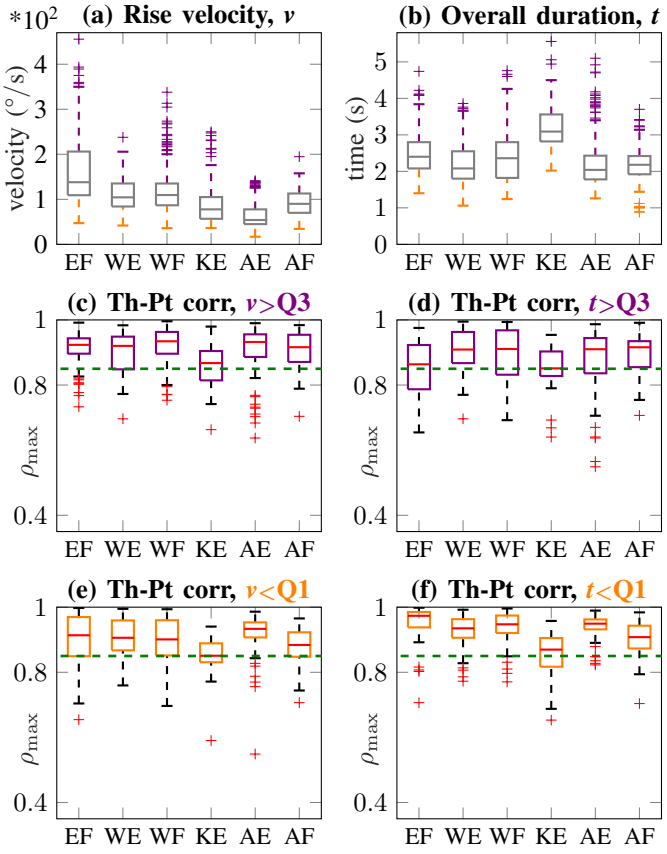

Fig. 7: Movements execution variability among different therapists in concentric phase velocity (a) and overall movement duration (b). Sub-figures (c) and (d) report therapist-patient cross-correlations obtained when velocity and duration are above Q3, respectively. On the other hand, (e) and (f) report what was obtained below Q1.

In conclusion, a last analysis takes into account how the variable execution of an exercise could have consequences on movements reproduction. Indeed, although the execution of a movement has been standardized as much as possible (e.g., by defining a reference posture), a variability among therapists actions needs to be considered. Rise velocity and movement duration have been selected as the parameters able to discriminate the difference in therapist movements, as it can be seen by the boxplots (e.g., looking at whiskers) in Fig. 7 (a) and (b). For the sake of the synthesis, here we focus the discussion of these results on the cross-correlation coefficient: $\rho_{\max}$ between the therapist and patient trajectories was computed for all cases in which these two parameters are greater than the third quartile (Q3) (Fig. 7 (c) and (d)) or less than the first quartile (Q1) (Fig. 7 (e) and (f)). Comparing all the permutations of movement velocity and duration, we concluded that each combination still ensure a median $\rho_{\max}$ above our acceptability criteria ($\rho_{\max} \geq 0.850$), although slower movements (lower rise velocity and longer duration) feature lower $\rho_{\max}$ values.

IV. State-of-the-Art Systems Comparison

Despite the differences among the state-of-the-art systems for FES control, we report a brief comparison with other works in Table V. The innovative aspect of our system is that the modulation of the stimulation intensity is performed using an event-driven technique, i.e., the ATC, which provides information about muscle activity without even sampling the sEMG signal. In this work, we investigated the versatility of our system in controlling the movements of different joints in a therapist-patient scenario by means of an extensive experimental campaign.

Comparing our system with the ones of the research group who published [22], [23], [54], we identified a potential

TABLE V: Comparison among recent state-of-the-art works for FES control.

Work	Control Mechanism	FES Modulation	Tested Movement	Tested Population	Th-Pt[1]	Evaluation Parameters
[35]	Hybrid FES exoskeleton	Pulse Width	Elbow Flexion	7 Healthy	No	94 % tracking error reduction and less 74 % control effort w.r.t. exoskeleton alone
[54]	Time-domain sEMG features	Pulse Width Frequency	Wrist Movements	6 Healthy	Yes	*Delay* $<$ 300 ms; $\rho_{\max} > 0.840$; *mean(SR)* = 92.5 %
[22]			Ankle Extension Ankle Flexion	6 Healthy	Yes	*Delay* $<$ 300 ms; $\rho_{\max} > 0.820$
[23]	Time-domain sEMG features	Pulse Width Frequency	Wrist Movements	6 Hemiplegic 1 Healthy	Yes	*Classification accuracy* $>$ 90 %; *mean(Delay)* = 270 ms; *mean*($\rho_{\max}$) = 0.840
[24]	Time-domain sEMG features	Pulse Amplitude	Wrist Movements	2 Healthy	No	*Classification accuracy* = 100 %; *mean(Delay)* = 600 ms (CCFES scenario)
[21]	sEMG envelope	Pulse Amplitude	Hand opening Grasping	1 Healthy	No	*mean(Classification accuracy)* = 81.72 %; *Delay* $>$ 2 s (CCFES scenario)
[55]	Angular velocity EMG modeling	Pulse Width	Ankle Flexion	10 Healthy 6 Drop Foot	No	*mean*($\rho_{\max}$) = 0.902 between FES-evoked EMG and natural EMG during gait
[56]	Angular velocity Flexion angle	Pulse Width	Ankle Flexion	10 Healthy	No	*Goodness of fit* = 77.87 % between real and reference ankle trajectories
This	ATC	Pulse Amplitude	Elbow, Wrist, Knee, Ankle extension/flexion	17 Healthy	Yes	*median(Delay)* = 660 ms–1080 ms; *median*($\rho_{\max}$) = 0.861–0.931; *SR* = 96.34 %–99.20 %

[1]Therapist-Patient approach

margin for improvements w.r.t. movement replication delays. Indeed, although our delays are comparable with [24] and lower than [21], their further decrement in system latency for obtaining a functional movement could improve the benefits of the mirror control in a rehabilitation scenario (i.e., promoting neural plasticity).

Looking at the system applicability, the main difference between [23] and our system architecture is the absence of a control platform (since the stimulation parameters definition is embedded in the acquisition device) and the use of a custom stimulator. From one side, a completely embedded system (with no GUI) could be appealing in implementing an autonomous and wearable system. Still, the user loses the possibility to supervise the ongoing stimulation actively. On the other side, dedicated FES solutions (e.g., stimulator algorithms and structure) optimize the stimulation effectiveness for a set of movements but reducing the application versatility of the system at different body parts.

Nevertheless, considering our case study, the proposed ATC-FES system shows good performance in controlling an induced motor activity (e.g., assessed by cross-correlation and successful rate parameters), featuring some of the highest values if compared with the figures of merit proposed in the other works.

V. Conclusions and Future Perspectives

This paper reports the experimental tests performed with our FES control system, detailing both the test protocol and the processing steps of the acquired data, in order to extract parameters for system evaluation. The use of this system allows a subject undergoing FES to replicate the voluntary movements of a subject from which muscle activity information is extracted using an event-driven approach. Compared to our latest FES-related paper [29], here we focused on the experimental part of our work, testing the system on a larger population of subjects while performing a wider set of movements. Moreover, we used a professional tool to capture subjects' limbs trajectories.

The lowest cross-correlation coefficient (median value) was found equal to 0.861 for knee extension, which also presents the highest replication delay, equal to 1.08 s. On the other hand, ankle extension and elbow flexion offers the highest movement correlation, with a median value equal to 0.931 and 0.923, respectively. A median replication delay value equal to 660 ms has been obtained for both ankle extension and ankle flexion, with the latter obtaining a successful rate equal to 99.2 %. The overall result of our testing campaign allow us to consider the proposed system a valid solution for therapist-controlled FES in the rehabilitation field.

Our next step is to use the proposed system to replicate more complex movements, e.g., reaching, to aim for application in the rehabilitation field to support Activities of Daily Living (ADL) [57]. To achieve this goal, we designed a more compact and wearable hardware [25] and, moving towards the use of our system for people with neural injuries, we are planning the study of muscle synergies to address muscle coordination impairments [58]. Moreover, we are aware that the current system is limited by modulation of stimulation intensity only. Further investigations will aim to use mathematical models to also modulate the stimulation frequency and pulse width to prevent muscle fatigue [59]. The main challenge would concern the development of a model for working in non-isometric contractions, still allowing the ATC employment in our system. Finally, we will have to investigate a an effective technique to analyze muscular activity directly from the stimulated muscles, thus exploiting this information for muscle fatigue monitoring [60] without excessively affecting the recorded signal quality.

References

[1] M. Johnston, M. Diab, S.-S. Kim, and S. Kirshblum, "Health literacy, morbidity, and quality of life among individuals with spinal cord injury," *The journal of spinal cord medicine*, vol. 28, pp. 230–40, 02 2005.

[2] R. Lo, O. Y. Cheng, M. Wong, W. Tang, K. Wong, J. Woo, and T. Kwok, "Handicap and its determinants of change in stroke survivors one-year follow-up study," *Stroke; a journal of cerebral circulation*, vol. 39, pp. 148–53, 02 2008.

[3] B. Armour, E. Courtney-Long, M. Fox, H. Fredine, and A. Cahill, "Prevalence and causes of paralysis-united states, 2013," *American journal of public health*, vol. 106, pp. e1–e3, 08 2016.

[4] S. Hatem, G. Saussez, M. Faille, V. Prist, X. Zhang, D. Dispa, and Y. Bleyenheuft, "Rehabilitation of motor function after stroke: A multiple systematic review focused on techniques to stimulate upper extremity recovery," *Frontiers in Human Neuroscience*, vol. 10, 09 2016.

[5] World Health Organization (WHO), Spinal cord injury. Accessed: December 17, 2021. [Online]. Available: https://www.who.int/news-room/fact-sheets/detail/spinal-cord-injury

[6] MS International Federation (MSIF), What is MS? Accessed: December 17, 2021. [Online]. Available: https://www.msif.org/about-ms/what-is-ms/

[7] K. Masani and M. Popovic, *Functional Electrical Stimulation in Rehabilitation and Neurorehabilitation*, 01 2011, pp. 877–896.

[8] HASOMED GmbH, *Operation Manual RehaStim2, RehaMove2 - User Guide*, September 2012.

[9] Y. Hara, "Rehabilitation with functional electrical stimulation in stroke patients," *International Journal of Physical Medicine and Rehabilitation*, vol. 01, 01 2013.

[10] C. Marquez Chin and M. Popovic, "Functional electrical stimulation therapy for restoration of motor function after spinal cord injury and stroke: a review," *BioMedical Engineering OnLine*, vol. 19, 05 2020.

[11] Z. Wang, L. Chen, W. Yi, B. Gu, S. Liu, X. An, M. Xu, H. Qi, F. He, B. Wan, and D. Ming, "Enhancement of cortical activation for motor imagery during BCI-FES training," in *2018 40th Annual International Conference of the IEEE Engineering in Medicine and Biology Society (EMBC)*, 2018, pp. 2527–2530.

[12] G. Buccino and L. Riggio, "The role of the mirror neuron system in motor learning," *Kinesiology 38(2006) 1:1-13*, 12 2013.

[13] L. Bi, A. G. Feleke, and C. Guan, "A review on EMG-based motor intention prediction of continuous human upper limb motion for human-robot collaboration," *Biomedical Signal Processing and Control*, vol. 51, pp. 113–127, 2019. [Online]. Available: https://www.sciencedirect.com/science/article/pii/S1746809419300473

[14] A. Benazzouz, R. Guilal, F. Amirouche, and Z. Slimane, "EMG Feature Selection for Diagnosis of Neuromuscular Disorders," 06 2019, pp. 1–5.

[15] N. Parajulli, N. Sreenivasan, P. Bifulco, M. Cesarelli, S. Savino, V. Niola, D. Esposito, T. Hamilton, G. Naik, U. Gunawardana, and G. Gargiulo, "Real-Time EMG Based Pattern Recognition Control for Hand Prostheses: A Review on Existing Methods, Challenges and Future Implementation," *Sensors*, vol. 19, p. 4596, 10 2019.

[16] K. Shima and K. Shimatani, "A new approach to direct rehabilitation based on functional electrical stimulation and EMG classification," 11 2016, pp. 1–6.

[17] S.-H. Lee, S. S. Kim, and B.-H. Lee, "Action observation training and brain-computer interface controlled functional electrical stimulation enhance upper extremity performance and cortical activation in patients with stroke: a randomized controlled trial," *Physiotherapy Theory and Practice*, pp. 1–9, 2020.

[18] H. Mao, Y. Li, L. Tang, Y. Chen, J. Ni, L. Liu, and C. Shan, "Effects of mirror neuron system-based training on rehabilitation of stroke patients," *Brain and Behavior*, vol. 10, no. 8, p. e01729, 2020.

[19] L. Fonseca, W. Tigra, B. Navarro, D. Guiraud, C. Fattal, A. Bó, E. Fachin-Martins, V. Leynaert, A. Gélis, and C. Azevedo-Coste, "Assisted grasping in individuals with tetraplegia: Improving control through residual muscle contraction and movement," *Sensors*, vol. 19, no. 20, 2019.

[20] A. Jasuja, V. Gupta, N. S. Sreenivasalu, M. Liu, J. Monz, J. S. Nir, and S. Bhasin, "Development of an extensible, wireless framework for personalized muscle rehabilitation," in *2019 IEEE Healthcare Innovations and Point of Care Technologies, (HI-POCT)*, 2019, pp. 17–20.

[21] E. M. Camilo, J. A. M. Gutiérrez, O. P. Ramírez, J. G. Martínez, A. V. Hernández, and L. L. Salas, "A Functional Electrical Stimulation Controller for Contralateral Hand Movements Based on EMG Signals," in *2020 17th International Conference on Electrical Engineering, Computing Science and Automatic Control (CCE)*, 2020, pp. 1–6.

[22] Z. Bi, X. Bao, H. Wang, X. Lv, and Z. Wang, "Prototype System Design and Experimental Validation of Gait-Oriented EMG Bridge for Volitional Motion Function Rebuilding of Paralyzed Leg," in *2019 IEEE 7th International Conference on Bioinformatics and Computational Biology (ICBCB)*, 2019, pp. 79–82.

[23] Z. Bi, Y. Wang, H. Wang, Y. Zhou, C. Xie, L. Zhu, H. Wang, B. Wang, J. Huang, X. Lü, and Z. Wang, "Wearable emg bridge—a multiple-gesture reconstruction system using electrical stimulation controlled by the volitional surface electromyogram of a healthy forearm," *IEEE Access*, vol. 8, pp. 137 330–137 341, 2020.

[24] Y. Chen, C. Dai, and W. Chen, "A Real-time EMG-controlled Functional Electrical Stimulation System for Mirror Therapy," 10 2019, pp. 1–4.

[25] F. Rossi, A. Mongardi, P. Motto Ros, M. Ruo Roch, M. Martina, and D. Demarchi, "Tutorial: A versatile bio-inspired system for processing and transmission of muscular information," *IEEE Sensors Journal*, vol. 21, no. 20, pp. 22 285–22 303, 2021.

[26] S. Sapienza, M. Crepaldi, P. Motto Ros, A. Bonanno, and D. Demarchi, "On Integration and Validation of a Very Low Complexity ATC UWB System for Muscle Force Transmission," *IEEE Transactions on Biomedical Circuits and Systems*, vol. 10, 05 2015.

[27] F. Rossi, P. Motto Ros, S. Sapienza, P. Bonato, E. Bizzi, and D. Demarchi, *Wireless Low Energy System Architecture for Event-Driven Surface Electromyography*, 05 2019, pp. 179–185.

[28] A. Mongardi, P. Motto Ros, F. Rossi, M. Ruo Roch, M. Martina, and D. Demarchi, "A Low-Power Embedded System for Real-Time sEMG based Event-Driven Gesture Recognition," in *2019 26th IEEE International Conference on Electronics, Circuits and Systems (ICECS)*, 2019, pp. 65–68.

[29] F. Rossi, P. Motto Ros, R. M. Rosales, and D. Demarchi, "Embedded Bio-Mimetic System for Functional Electrical Stimulation Controlled by Event-Driven sEMG," *Sensors*, vol. 20, no. 5, p. 1535, Mar 2020. [Online]. Available: http://dx.doi.org/10.3390/s20051535

[30] F. Rossi, P. Motto Ros, S. Cecchini, A. Crema, S. Micera, and D. Demarchi, "An Event-Driven Closed-Loop System for Real-Time FES Control," 11 2019, pp. 867–870.

[31] C. J. De Luca, *Surface Electromyography: Detection and Recording*. DelSys Incorporated, 2002.

[32] Apollo3 blue. Accessed: December 17, 2021. [Online]. Available: https://ambiq.com/apollo3-blue/

[33] B. Kuberski, *ScienceMode2, RehaStim2 Stimulation Device, Description and Protocol*.

[34] Vicon. Accessed: December 17, 2021. [Online]. Available: https://www.vicon.com/

[35] D. Wolf, N. Dunkelberger, C. McDonald, K. Rudy, C. Beck, M. O'Malley, and E. Schearer, "Combining functional electrical stimulation and a powered exoskeleton to control elbow flexion," 11 2017, pp. 1–2.

[36] C. Lynch, D. Sayenko, and M. Popovic, "Co-contraction of antagonist muscles during knee extension against gravity: Insights for functional electrical stimulation control design," *Conference proceedings : ... Annual International Conference of the IEEE Engineering in Medicine and Biology Society. IEEE Engineering in Medicine and Biology Society. Conference*, vol. 2012, pp. 1843–6, 08 2012.

[37] W. Huo, V. Arnez-Paniagua, M. Ghedira, Y. Amirat, J.-M. Gracies, and S. Mohammed, "Adaptive fes assistance using a novel gait phase detection approach," in *2018 IEEE/RSJ International Conference on Intelligent Robots and Systems (IROS)*, 2018, pp. 1–9.

[38] S.-Y. Ha, J.-H. Han, Y. Ko, and Y.-H. Sung, "Ankle exercise with functional electrical stimulation affects spasticity and balance in stroke patients," *Journal of Exercise Rehabilitation*, vol. 16, pp. 496–502, 12 2020.

[39] J. Soucie, C. Wang, A. Forsyth, S. Funk, M. Denny, K. Roach, and D. Boone, "Range of motion measurements: Reference values and a database for comparison studies," *Haemophilia : the official journal of the World Federation of Hemophilia*, vol. 17, pp. 500–7, 11 2010.

[40] J. Ryu, W. P. Cooney, L. J. Askew, K.-N. An, and E. Y. Chao, "Functional ranges of motion of the wrist joint," *The Journal of Hand Surgery*, vol. 16, no. 3, pp. 409–419, 1991. [Online]. Available: https://www.sciencedirect.com/science/article/pii/036350239190006W

[41] Università degli Studi di Torino - Comitato di Bioetica dell'Ateneo. Accessed: December 17, 2021. [Online]. Available: https://www.unito.it/ricerca/strutture-e-organi-la-ricerca/comitato-di-bioetica-dellateneo

[42] Vicon Nexus User Guide. Accessed: December 17, 2021. [Online]. Available: https://docs.vicon.com/display/Nexus211/Vicon+Nexus+User+Guide

[43] Plug-in Gait Reference Guide. Accessed: December 17, 2021. [Online]. Available: https://docs.vicon.com/display/Nexus211/Plug-in+Gait+Reference+Guide

[44] SENIAM project. Accessed: December 17, 2021. [Online]. Available: http://www.seniam.org/

[45] HASOMED GmbH, *RehaMove, Functional electrical stimulation - FES applications*, June 2015.

[46] Electrode placement and functional movement. Accessed: December 17, 2021. [Online]. Available: https://www.axelgaard.com/Education/Electrode-Placement-and-Functional-Movement

[47] Cardinal Health. Kendall H124SG Electrodes. Accessed: December 17, 2021. [Online]. Available: https://www.cardinalhealth.co.uk/en_gb/medical-products/patient-care/electrocardiography/adult-monitoring-electrodes/general-monitoring-ecg-electrodes/long-term-electrodes/kendall-electrodes-h124sg.html

[48] FIAB products. Accessed: December 17, 2021. [Online]. Available: https://www.fiab.it/prodotti.php

[49] D. Jessop and M. Pain, "Maximum velocities in flexion and extension actions for sport," *Journal of Human Kinetics*, vol. 50, 03 2016.

[50] Nexus. Accessed: December 17, 2021. [Online]. Available: https://www.vicon.com/software/nexus/

[51] A. Do, P. Wang, C. King, A. Abiri, and Z. Nenadic, "Brain-computer interface controlled functional electrical stimulation system for ankle movement," *Journal of neuroengineering and rehabilitation*, vol. 8, p. 49, 08 2011.

[52] A. Vette, K. Masani, and M. Popovic, "Time Delay from Muscle Activation to Torque Generation during Quiet Stance: Implications for Closed-Loop Control via FES," *Biomed Tech*, vol. 53, 01 2008.

[53] R. J. Downey, M. Merad, E. J. Gonzalez, and W. E. Dixon, "The time-varying nature of electromechanical delay and muscle control effectiveness in response to stimulation-induced fatigue," *IEEE Transactions on Neural Systems and Rehabilitation Engineering*, vol. 25, no. 9, pp. 1397–1408, 2017.

[54] Y.-X. Zhou, H.-P. Wang, X.-P. Cao, Z.-Y. Bi, Y.-J. Gao, X.-B. Chen, X.-Y. Lü, and Z.-G. Wang, "Electromyographic bridge—a multi-movement volitional control method for functional electrical stimulation: prototype system design and experimental validation," in *2017 39th Annual International Conference of the IEEE Engineering in Medicine and Biology Society (EMBC)*, 2017, pp. 205–208.

[55] Y. Li, X. Yang, Y. Zhou, J. Chen, M. Du, and Y. Yang, "Adaptive stimulation profiles modulation for foot drop correction using functional electrical stimulation: a proof of concept study," *IEEE journal of biomedical and health informatics*, vol. 25, no. 1, pp. 59–68, 2020.

[56] S. Carvalho, A. Correia, J. Figueiredo, J. M. Martins, and C. P. Santos, "Functional electrical stimulation system for drop foot correction using a dynamic narx neural network," *Machines*, vol. 9, no. 11, p. 253, 2021.

[57] A. Cuesta-Gómez, M. Carratalá-Tejada, F. Molina-Rueda, and J. C. Miangolarra-Page, "Functional electrical stimulation improves reaching movement in the shoulder and elbow muscles of stroke patients: A three-dimensional motion analysis," *Restorative neurology and neuroscience*, vol. 37, no. 3, pp. 231–238, 2019.

[58] J. Lim, T. Lim, J. Lee, J. Sim, H. Chang, B. Yoon, and H. Jung, "Patient-specific functional electrical stimulation strategy based on muscle synergy and walking posture analysis for gait rehabilitation of stroke patients," *Journal of International Medical Research*, vol. 49, no. 5, p. 03000605211016782, 2021.

[59] B. D. Doll, N. A. Kirsch, X. Bao, B. E. Dicianno, and N. Sharma, "Dynamic optimization of stimulation frequency to reduce isometric muscle fatigue using a modified hill-huxley model," *Muscle & nerve*, vol. 57, no. 4, pp. 634–641, 2018.

[60] C. Klauer, S. Ferrante, E. Ambrosini, U. Shiri, F. Dähne, I. Schmehl, A. Pedrocchi, and T. Schauer, "A patient-controlled functional electrical stimulation system for arm weight relief," *Medical engineering & physics*, vol. 38, no. 11, pp. 1232–1243, 2016.

Andrea Prestia (GSM'21) received both his Bachelor and Master degrees in biomedical engineering from Politecnico di Torino, Turin, Italy, in 2018 and 2020, respectively.

He is a member of Micro and Nano Electronic System (MiNES) research group and his research interests include the design of electronic systems for biomedical applications.

Fabio Rossi (M'20) received both his Bachelor and Master degrees in Biomedical Engineering from Politecnico di Torino, Turin, Italy, in 2015 and 2017, respectively.

He started his Ph.D. studies in electronic engineering since November 2018, at Politecnico di Torino, Department of Electronics and Telecommunications. Research interests are focused on design of low-power systems for medical bio-electronic applications. Since 2016 he is member of Micro and Nano Electronic System (MiNES) research group.

Andrea Mongardi (M'18) received both his Bachelor in electronic engineering and the Master in electronic engineering, embedded systems specialization, from Politecnico di Torino, Turin, Italy, in 2017 and 2019, respectively.

Since November 2020 he is a PhD candidate at Politecnico di Torino, Department of Electronics and Telecommunications, focusing on the design of low power embedded systems for sEMG acquisition, and member of the Micro and Nano Electronic Systems (MiNES) Laboratory.

Paolo Motto Ros (M'16) received the Engineering and Ph.D. degrees in electronic engineering from the Politecnico di Torino (IT), in 2005 and 2009, respectively.

He is Senior Post-Doctoral Researcher and Adjunct Professor at Politecnico di Torino (IT), Dipartimento di Elettronica e Telecomunicazioni, with the MiNES (Micro&Nano Electronic Systems) group. From 2009 to 2012, he was with Politecnico di Torino as Postdoc Researcher (jointly with, 2009–2013, Istituto Nazionale Fisica Nucleare, INFN, IT). From 2012 to 2019, he was with Istituto Italiano di Tecnologia as Senior (since 2014) Postdoc Researcher. He counts more than 60 publications; current research interests include: event-driven digital integrated circuits, architectures, and systems; low-power smart sensor networks; bio-inspired electronics; biomedical and humanoid robotic applications.

Dr. Motto Ros is member of the IEEE CAS Society. He was member of the organizing staff of the IEEE BioCAS 2017 conference, and member of the organizing committee of the IEEE ICECS 2019 conference and the FoodCAS Satellite Event at the IEEE ISCAS 2021 conference. He is guest editor of MDPI Sensors and topic editor of Frontiers in Neurorobotics.

Massimo Ruo Roch (M'20) received the M.S and Ph.D. degrees in electrical engineering from the Politecnico di Torino, Italy, in 1989 and 1993, respectively.

He is currently an Assistant Professor from the VLSI-Lab Group, Politecnico di Torino. His research interests include VLSI design and implementation of architectures for digital signal processing, communications, embedded systems design, smart systems with distributed intelligence, logic in memory architectures, and cad tools for nanotechnology based architectures. He is co-author of more than 60 papers.

Maurizio Martina (M'04, SM'15) received the M.S. and Ph.D. degrees in electrical engineering from the Politecnico di Torino, Italy, in 2000 and 2004, respectively.

He is currently an Associate Professor from the VLSI-Lab Group, Politecnico di Torino. His research interests include VLSI design and implementation of architectures for digital signal processing, video coding, communications, artificial intelligence, machine learning, and event-based processing. He edited one book and published three book chapters on VLSI architectures and digital circuits for video coding, wireless communications, and error correcting codes. He has more than 100 scientific publications and is coauthor of two patents.

Prof. Martina is currently an Associate Editor of the IEEE Transactions on Circuits and Systems—I: Regular Papers. He had been part of the Organizing and Technical Committee of several international conferences, including BioCAS 2017, ICECS 2019, and AICAS 2020. He is also the Counselor of the IEEE Student Branch at the Politecnico di Torino and a Professional Member of IEEE HKN.

Danilo Demarchi (M'10-SM'13) received Engineering Degree and Ph.D. in electronics engineering from Politecnico di Torino, Italy, in 1991 and 1995, respectively.

Full position as Associate Professor at Politecnico di Torino, Department of Electronics and Telecommunications, Turin, Italy. Visiting Professor at Tel Aviv University (2018-2021) and at EPFL Lausanne (2019). Visiting Scientist at MIT and Harvard Medical School (2018). Author and co-author of 5 patents and more than 250 international scientific publications.

Prof. Demarchi is the leader of the MiNES (Micro&Nano Electronic Systems) Laboratory at Politecnico di Torino, Member of the BioCAS Technical Committee, Associate Editor of IEEE Sensors Journal and of the Springer Journal BioNanoScience, Member of IEEE Sensors Council, General Chair of IEEE BioCAS 2017 and founder of the IEEE FoodCAS Workshop (Circuits and Systems for the Food Chain).